PLANT SCIENCES

Blocking the isoflavone chemoreceptor in *Phytophthora sojae* to prevent disease

Peiyun Ji[1]†, Yazhou Bao[2]†‡, Hao Zhou[1], Yong Pei[1], Wen Song[1], Kangmiao Ou[3], Zijin Qiao[1], Jierui Si[1], Zengtao Zhong[3], Xia Xu[4], Tao Huang[4], Danyu Shen[1], Zhiyuan Yin[1]*, Daolong Dou[1,2]*

Inhibiting pathogen chemotaxis is a promising strategy for reducing disease pressure. However, this strategy is currently in the proof-of-concept stage. Here, *Phytophthora sojae* was used as a model, as its biflagellated zoospores could sense genistein, a soybean root exudate, to navigate host and initiate infection. We identify *P. sojae* IRK1 (isoflavone-insensitive receptor kinase 1) as a receptor for genistein, with PsIRK2 functioning as a coreceptor that enhances the binding affinity of PsIRK1 to genistein and regulates chemotaxis by phosphorylating G protein α subunit. Last, we identify an antagonist, esculetin, which disrupts the PsIRK1-genistein interaction, thereby preventing *P. sojae* infection by repelling zoospores. Our findings reveal the mechanism by which *P. sojae* senses host genistein and demonstrate a strategy for disease prevention by targeting the chemoreceptor.

INTRODUCTION

Chemotaxis is crucial for flagellated pathogens to initiate infection, as this process permits these pathogens to find their hosts. Blocking chemotaxis process, which is currently in the proof-of-concept stage, is a promising strategy to reduce disease pressure (*1*, *2*). Oomycetes belong to the Stramenopila and produce biflagellated zoospores as the primary source of infection, which show chemotaxis toward exudates of host plants (*3*, *4*). For instance, *Phytophthora sojae*, the primary causal agent of soybean root rot that causes an annual global economic loss of $1 to 2 billion (*5*), finds soybean roots mainly by sensing isoflavones including genistein (GEN) and daidzein (DAI) in the rhizosphere (*6*). Blocking the chemoreceptor is an efficient strategy to inhibit chemotaxis, yet the mechanism by which *P. sojae* zoospores sense GEN remains largely elusive.

In other eukaryotes, such as fungi and mammalian cells, chemotaxis or chemotropism is mediated by cell-surface G protein–coupled receptors (GPCRs) (*7*, *8*). *P. sojae* has approximately 60 GPCR(-like) proteins (*9*). Silencing of *PsGK4* (*GPCR-PIPK 4*) impairs zoospore chemotaxis toward DAI (*10*). Silencing the G protein α subunit–encoding gene *PsGPA1* lead to absent of chemotaxis (*11*). However, PsGK4 seemed unable to interact with PsGPA1 (*10*), raising questions about the chemotaxis signal transduction mechanism from the extracellular environment to PsGPA1. Besides GPCRs, more than 100 receptor-like kinases (RLKs) were also found in the *P. sojae* genome (*12*), including the leucine-rich repeat (LRR) family which is the largest family in plants (*13*). Knockout mutants of five *P. sojae LRR-RLKs* [here referred to as *Isoflavone-insensitive Receptor Kinases* (*IRKs*)] showed impaired zoospore chemotaxis toward soybean isoflavones, and these five PsIRKs could interact with PsGPA1 (*14*). In plants, RLKs phosphorylate G protein α subunits to transduce signal and regulate plant development and immunity (*15*–*18*). These findings prompt us to investigate whether PsIRKs are chemoreceptors for soybean isoflavones.

Here, we report a strategy to prevent disease by blocking the isoflavone chemoreceptor in *P. sojae*. We demonstrate that PsIRK1 is the receptor for GEN, the primary bioactive isoflavone in soybean root exudates that attracts *P. sojae* zoospores. PsIRK2 functions as a coreceptor, enhancing the binding of GEN to PsIRK1 and phosphorylating PsGPA1 to specifically transmit chemotaxis signaling. Esculetin (ESC), a GEN analog that does not affect the *Rhizobium*-soybean symbiosis, repulses *P. sojae* zoospores by competitively binding to PsIRK1 in place of GEN and exhibits promising effect on controlling damping off disease caused by *P. sojae*.

RESULTS

PsIRK1 and PsIRK2 are responsible for chemotaxis to GEN

Blocking chemoreceptors is an effective way to inhibit chemotaxis. Therefore, in this study, we aimed to identify the receptors for GEN (GEN) and DAI, the two primary isoflavones secreted into the soybean rhizosphere. Supplemental movies showed that both GEN and DAI induced violent aggregation of *P. sojae* zoospores in the capillary tube within 6 min (fig. S1 and movies S1 and S2). Notably, GEN was found to be notably more potent than DAI, consistent with the previous report (*19*). Chemotaxis phenotypes were then determined in five knockout mutants of *PsIRKs*, which were previously shown to exhibit reduced attraction to isoflavone-containing agarose plugs (*14*). Both GEN and DAI successfully attracted wild-type (WT) *P. sojae* zoospores into the capillary tube and induced rapid encystment (movies S1 and S2). However, zoospores of Δ*PsIRK4* and Δ*PsIRK5* mutants kept swimming without encystment, resulting in fewer zoospores aggregating in the capillaries (movies S3 to S6). This suggests that PsIRK4 and PsIRK5 are likely involved in GEN- and DAI-induced encystment but not the chemotaxis. In contrast, GEN induced normal encystment of Δ*PsIRK1* and Δ*PsIRK2* zoospores but attracted remarkedly fewer zoospores into the capillary tube (movies S7 to S10). Similarly, DAI attracted fewer zoospores of Δ*PsIRK2* and Δ*PsIRK3* mutants (movies S9 to S12). These results indicate that PsIRK2/3 and PsIRK1/2 are responsible for chemotaxis to DAI and GEN, respectively.

To further investigate their roles in chemotaxis, we examined Ca^{2+} influx, a typical cellular response triggered by GEN and DAI

[1]Department of Plant Pathology, Nanjing Agricultural University, Nanjing 210095, China. [2]Academy for Advanced Interdisciplinary Studies, Nanjing Agricultural University, Nanjing 210095, China. [3]College of Life Sciences, Nanjing Agricultural University, Nanjing 210095, China. [4]Hefei Kejing Biotechnology Co., Ltd., Hefei 230061, China.
*Corresponding author. Email: zyin@njau.edu.cn (Z.Y.); ddou@njau.edu.cn (D.D.)
†These authors contributed equally to this work.
‡Present address: The Nanjing Engineering Research Center for Peanut Genetic Engineering Breeding and Industrialization, School of Food Science, Nanjing Xiaozhuang University, Nanjing 211171, China.

(*20*). The Ca^{2+} levels in WT zoospores increased five- or eightfold after a 5-min treatment with 10 nM GEN or DAI, respectively, compared to the dimethyl sulfoxide (DMSO) control. In contrast, zoospores of Δ*PsIRK1* and Δ*PsIRK2* showed unchanged Ca^{2+} levels upon GEN treatment (Fig. 1A and fig. S2, A and B). Likewise, DAI treatment failed to trigger Ca^{2+} increase in Δ*PsIRK2* and Δ*PsIRK3* mutants (fig. S2B). Moreover, both GEN and DAI stimulated the mitogen-activated protein kinase (MAPK) activation in WT zoospores within 10 and 5 min, respectively (fig. S2, C and D). However, GEN- and DAI-triggered MAPK activation was blocked in Δ*PsIRK2*, while the Δ*PsIRK1* mutant failed to activate the MAPK cascade after GEN treatment but not DAI (Fig. 1B and fig. S2E). The Δ*PsIRK3* mutant showed no significant difference compared to WT upon treatment with neither GEN nor DAI.

Next, we generated a Δ*PsIRK1/2* double mutant (fig. S3). Zoospores of the Δ*PsIRK1/2* double mutant displayed the same chemotaxis phenotype as Δ*PsIRK1* and Δ*PsIRK2* (movies S13 and S14). To look for changes in virulence of these mutants, we used root dipping and hypocotyl inoculation assays, and we found that ΔPsIRK1, ΔPsIRK2, and ΔPsIRK1/2 mutants showed impaired virulence compared with WT in root dipping assays (Fig. 1, C and D, and fig. S3E) but not in hypocotyl inoculation. These findings suggest that PsIRK1 and PsIRK3 are specifically responsible for GEN and DAI respectively, with PsIRK2 functioning downstream.

PsIRK2 enhances the binding affinity of PsIRK1 to GEN

To further determine the cognate receptors for GEN and DAI, recombinant extracellular domain (ECD) proteins of PsIRK1, PsIRK2, and PsIRK3 were successfully expressed by yeast and purified (fig. S4A). Microscale thermophoresis (MST) assays revealed that $PsIRK1^{ECD}$ bound specifically to GEN with a K_D value of 20.4 μM (Fig. 2A), whereas $PsIRK3^{ECD}$ specifically bound to DAI with a K_D value of 69.0 μM (fig. S4B). Despite the impaired chemotaxis phenotypes observed in the Δ*PsIRK2* mutant, no binding was detected between $PsIRK2^{ECD}$ and either GEN or DAI (Fig. 2A and fig. S4B). This finding prompts us to hypothesize that PsIRK2 forms complexes with PsIRK1 or PsIRK3 to regulate chemotaxis. To test this hypothesis, PsIRK2 was coexpressed with PsIRK1/2/3/4/5, respectively, in *Nicotiana benthamiana* leaves by agroinfiltration for coimmunoprecipitation (Co-IP) assays. The results demonstrated that PsIRK2 could interact with PsIRK1 and PsIRK3 but not with PsIRK4 or PsIRK5 (Fig. 2B). Interactions between $PsIRK1^{ECD}$ and $PsIRK2^{ECD}$ or $PsIRK3^{ECD}$ were further confirmed by Co-IP and glutathione-*S*-transferase (GST) pulldown assays, which were specifically enhanced by GEN and DAI treatment, respectively (Fig. 2, C to E, and fig. S4, C to E). In addition, MST assay showed that the affinity between $PsIRK1^{ECD}$ and GEN was improved to a K_D value of 0.72 μM in the presence of $PsIRK2^{ECD}$, which represents 17-fold increase (Fig. 2F). Similarly, $PsIRK2^{ECD}$ also promoted the affinity between $PsIRK3^{ECD}$ and DAI

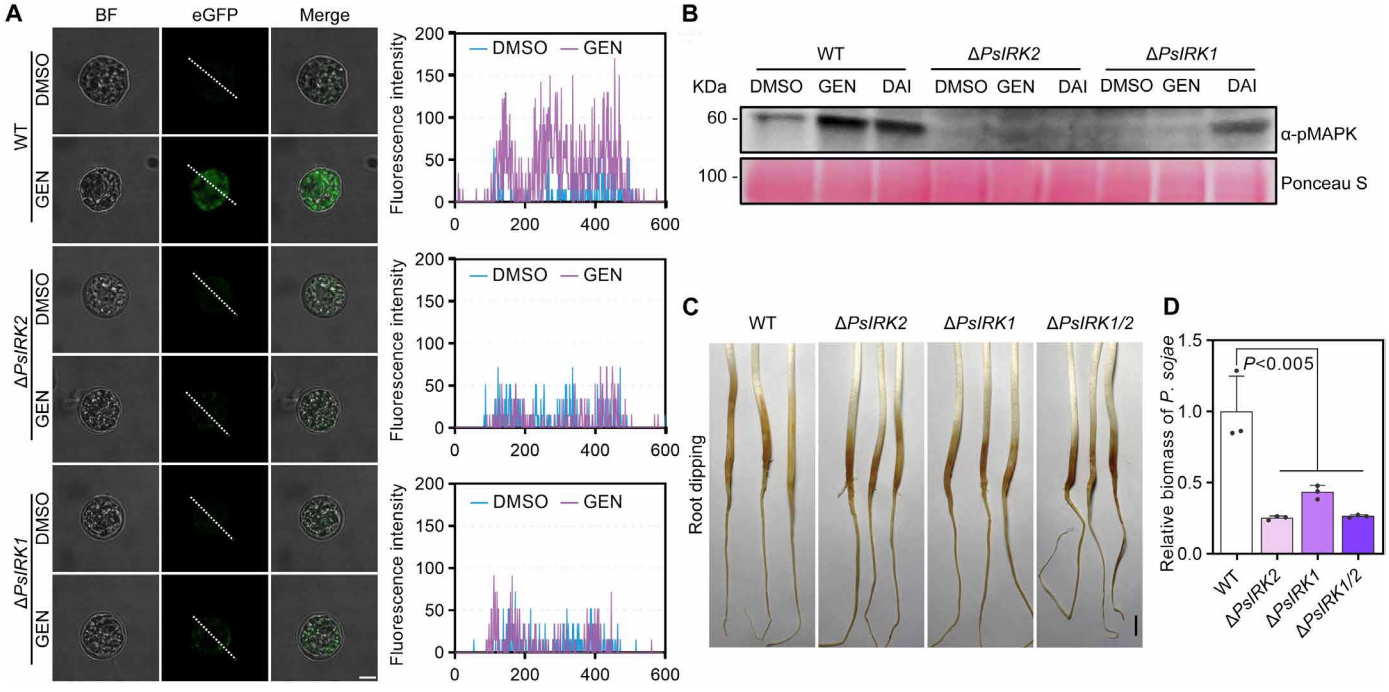

Fig. 1. PsIRK1 and PsIRK2 are responsible for chemotaxis to GEN. (**A**) Immunofluorescence staining of intracellular Ca^{2+} in zoospores of wild-type (WT), Δ*PsIRK1*, and Δ*PsIRK2* strains. Zoospores were treated with GEN or DMSO for 5 min before staining with Fluo-4 AM to detect Ca^{2+} influx. Fluorescence was visualized using laser confocal microscopy at 100× magnification (left). Scale bar, 5 μm. Quantitative analysis of the fluorescence intensity along the dotted line (left) using Zeiss ZEN software (right). (**B**) GEN induces MAPK activation in zoospores of WT, Δ*PsIRK1*, and Δ*PsIRK2* strains. The zoospore suspension was treated with GEN for 10 min, or with DAI for 5 min as a control. MAPK activation was analyzed by immunoblotting with the α-pMAPK antibody. Protein loading was verified using Ponceau S staining. (**C** and **D**) Δ*PsIRK1* and Δ*PsIRK2* mutants show reduced virulence due to decreased chemotaxis. Roots of susceptible etiolated soybean hypocotyls (cultivar Hefeng47) were dipped into zoospore suspension of WT, Δ*PsIRK1*, and Δ*PsIRK2* for 30 min at a concentration of 10^5/ml. Lesion lengths were assessed 48 hours postinoculation (hpi). Relative biomass of WT, Δ*PsIRK1*, and Δ*PsIRK2* in infected etiolated soybean hypocotyls was measured by quantitative reverse transcription PCR and normalized to that of WT ($n = 3$ biologically independent experiments). Statistical significance was determined by one-way analysis of variance (ANOVA) followed by Tukey's test, $P < 0.01$. Error bars indicate the mean fold changes with SD.

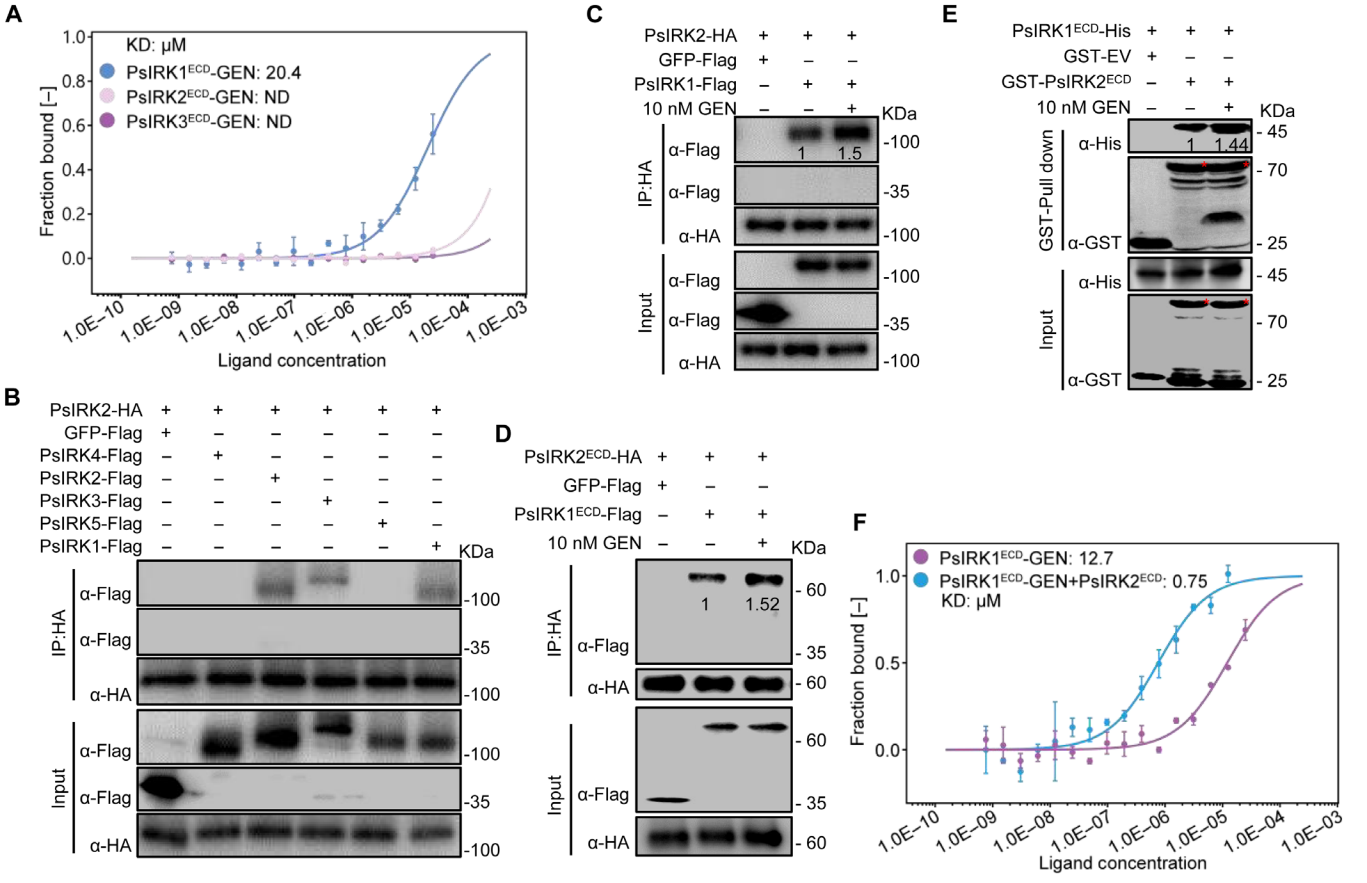

Fig. 2. PsIRK2 enhances the binding affinity of PsIRK1 to GEN. (**A**) Microscale electrophoresis (MST) analysis of GEN binding to PsIRK1^{ECD}. (**B**) PsIRK2 interacts with PsIRK1 and PsIRK3 in Co-IP assay. Proteins were transiently expressed in *N. benthamiana* leaves via agroinfiltration. (**C** and **D**) GEN promotes the interaction between PsIRK1 and PsIRK2 in Co-IP assay, as well as between PsIRK1^{ECD} and PsIRK2^{ECD}. The 10 nM GEN or equal volume of DMSO was infiltrated in *N. benthamiana* leaves 30 min before proteins extraction. (**E**) GEN promotes the interaction between PsIRK1^{ECD} and PsIRK2^{ECD} in pulldown assay. (**F**) MST profiles show that PsIRK2^{ECD} enhances the binding affinity of PsIRK1^{ECD} to GEN.

by about ninefold (fig. S4F). Collectively, these findings above demonstrate that PsIRK1 and PsIRK3 are the receptors of GEN and DAI respectively, while PsIRK2 may acts as a coreceptor that facilitates ligand binding of PsIRK1 and PsIRK3. Given that GEN is considerably more potent than DAI (movie S1 and S2) (*19*), we focused on the mechanism of GEN hereafter.

We found that PsIRK2 constitutively formed homodimers, which raised the question of the interaction model between PsIRK1 and PsIRK2 when sensing GEN. First, we carried out GST pulldown assays to detect whether PsIRK1 form homodimers before and after the GEN treatment. The result showed that PsIRK1 did not form homodimers even with the presence of GEN (fig. S5, A and B). We further conducted the size exclusion chromatography assay to detect the complex between PsIRK1 and PsIRK2. The result showed that the peak time of the curve delayed after adding PsIRK1 and PsIRK2 together, but adding GEN to the system had no effect on the peak time (fig. S5, C to E). This result indicated that PsIRK1 interacted with PsIRK2 without changing the protein numbers after GEN treatment. In plants, the RLK SOBIR1 (SUPPRESSOR OF BIR1-1) also constitutively forms homodimers, which allows basal activation of its kinase domain (KD) by cross-phosphorylation (*21*). Collectively, these findings suggest that the PsIRK1/PsIRK2 complex might be activated by conformational changes, and PsIRK2 homodimers possibly allow basal activation of its KD (fig. S5F).

PsIRK2 regulates chemotaxis by phosphorylating the G protein α subunit

To investigate how PsIRKs regulate chemotaxis signaling, we noticed the *P. sojae* G protein α subunit (PsGPA1), which was previously proven to be indispensable for chemotaxis to isoflavones and interact with PsIRKs (*11*, *14*). Thus, we examined the kinase activity of these PsIRKs using in vitro kinase assays. Among the five recombinant proteins of the KDs, only PsIRK2^{KD} exhibited a clear autophosphorylation activity and was capable to phosphorylate PsGPA1, while the kinase-dead mutant PsIRK2$^{KD\text{-}K501E}$ did not (Fig. 3, A and B, and fig. S6). The phosphorylated PsGPA1 proteins were then subjected to mass spectrometry and five phosphorylation sites (T^{111}, Y^{154}, T^{169}, T^{194}, and Y^{198}) were identified (fig. S6). To investigate their roles in chemotaxis, we generated a quintuple-point mutant (*PsGPA1*^{5A}), which showed clearly reduced phosphorylation level mediated by PsIRK2^{KD} (Fig. 3C).

Next, we generated the Δ*PsGPA1* knockout mutant and *PsGPA1*^{5A}, a quintuple-point dephosphorylated mutant, in *P. sojae* strain P6497 through CRISPR-Cas9 (fig. S7, A to D). Both mutants exhibited no

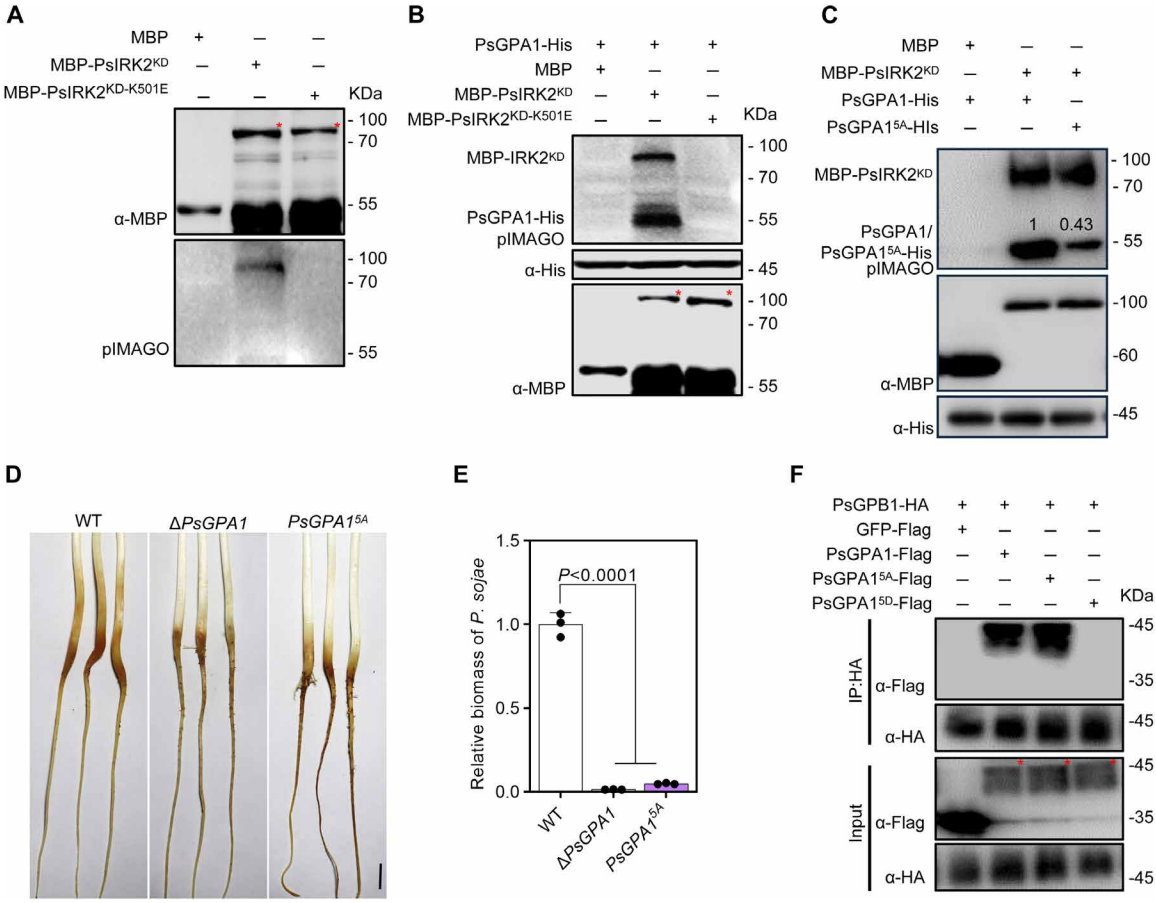

Fig. 3. PsIRK2 regulates chemotaxis by phosphorylating the G protein α subunit. (**A**) The kinase domain (KD) of PsIRK2 exhibits autophosphorylation activity in vitro. The pIMAGO-biotin phosphoprotein detection kit was used to probe the phosphorylated blots. (**B**) PsGPA1 is phosphorylated by PsIRK2^{KD} in vitro. (**C**) The quintuple-point mutant of candidate phosphorylation sites on PsGPA1 shows reduced phosphorylation level. (**D** and **E**) Δ*PsGPA1* and *PsGPA1*^{5A} mutants show reduced virulence. Ordinary one-way ANOVA with Dunnett's multiple comparisons tests were used, $P < 0.01$. Error bars indicate the mean fold changes with SD. (**F**) The phosphorylation mimic PsGPA1^{5D} does not interact with the G protein β subunit (PsGPB1) in Co-IP assay.

significant difference in the growth rate on V8 and virulence when inoculated with mycelium (fig. S7, E to M). However, the Δ*PsGPA1* mutant displayed a markedly decreased cyst germination phenotype, which led to its low virulence when inoculated with zoospore suspensions compared with WT and *PsGPA1*^{5A} strains (fig. S7, I, J, L, and M). Likewise, Δ*PsGPA1* zoospores showed an increased turn around frequency, while *PsGPA1*^{5A} mutant did not (fig. S7K). Both Δ*PsGPA1* and *PsGPA1*^{5A} zoospores severely impaired on zoospore chemotaxis to GEN and DAI (movies S15 to S18). In addition, biomass of the two mutants in infected roots was markedly reduced following zoospore inoculation by root dipping (Fig. 3, D and E).

In plants, phosphomimetic Gα proteins fail to interact with Gβ (*17*). Therefore, we also evaluated the interactions between G protein β subunit (PsGPB1) and PsGPA1, PsGPA1^{5A}, or PsGPA1^{5D} (phosphorylation mimic mutation) by Co-IP assay. The result showed that PsGPA1 and PsGPA1^{5A} but not PsGPA1^{5D} interacted with PsGPB1 (Fig. 3F), suggesting that phosphorylation of PsGPA1 leads to dissociation of the G protein ternary complex. In summary, these results indicate that PsIRK2 phosphorylate PsGPA1 at five candidate sites, which are specifically responsible for zoospore chemotaxis, but no other processes mediated by PsGPA1.

Antagonist ESC prevents *P. sojae* infection by repelling zoospores

To explore antagonists that disturb chemotaxis toward GEN, we performed a virtual screening to predict PsIRK1-binding compounds. A previous study reported that a simple coumarin could repel zoospores of different *P. sojae* strains (*19*). Since simple coumarins have structures similar to GEN but with lower molecular weights, a set of 461 simple coumarins was selected for virtual screening (table S3). After docking, the predicted affinity ranged −6.93 to −4.93 kcal/mol. Using −5.80 kcal/mol as the threshold, we filtered the compounds down to 187, of which 14 were available and subsequently tested for repellent activity (table S3). ESC, scopoletin, 7-ethoxycoumarin, and 6-hydroxycoumarin were shown to repel *P. sojae* zoospores, while only ESC inhibited GEN-induced chemotaxis in a PsIRK1-denpendent manner (movies S19 and S20 and fig. S8E). Thus, further work was focused on ESC, which was originally isolated from sweet potato roots with black rot (*22*). To uncover the mechanism of ESC, we determined the interaction between PsIRK1^{ECD} and ESC by MST assay. The result showed that PsIRK1^{ECD} binds to ESC with a K_D value of 13.8 μM, which was unaffected by the presence of PsIRK2^{ECD} (Fig. 4B). Furthermore, ESC markedly reduced

the affinity between PsIRK1^{ECD} and GEN to a KD value of 333.4 μM, representing a 20-fold decrease (Fig. 4C). These results suggest that ESC disturbs zoospore chemotaxis toward GEN by competitively binding PsIRK1.

We also tested additional effects of ESC on *P. sojae*. ESC did not inhibit the mycelial growth of *P. sojae* at a concentration of 100 μM, nor did it affect the cyst germination rate, indicating that ESC does not have a direct inhibitory effect on the pathogen (fig. S8, A to D). Pretreatment of etiolated soybean hypocotyls with ESC for 30 min did not affect the infection when *P. sojae* zoospores were directly inoculated on hypocotyls (Fig. 4, D and E). In contrast, in root dipping assays, where chemotaxis is critical for infection, ESC treatment significantly reduced *P. sojae* biomass in soybean tissues. Since ESC did not influence the growth of soybean (fig. S8G), we also carried out pot experiments to further verify effect of ESC on preventing *P. sojae* infection. Pretreatment with ESC for 30 min before zoospore inoculation increased the survival rate of soybean seedlings to 60%, nearly three times higher than the DMSO control (Fig. 4, F and G). These findings support that ESC could prevent soybean root rot by disorienting *P. sojae* zoospores.

To further evaluate ESC as a potential agent for *P. sojae* prevention, we tested its effects on *Sinorhizobium fredii* strain CCBAU45436, a dominant fast-growing rhizobium that forms nitrogen-fixing root nodules on soybean and senses GEN as symbiotic signal (*23*). The logistic growth curve showed that ESC did not affect the growth of *S. fredii* (fig. S8F). To determine the effect of ESC on symbiotic performance of *S. fredii*, number of nodules, nitrogenase activity, and height and fresh weight of soybean aerial part were measured at 28 days postinoculation. No significant difference was observed in height and fresh weight after adding ESC to the root compared to mock (fig. S8, G to I). *S. fredii* uses NodD as receptor to sense GEN, promoting the expression of nod genes. To determine whether ESC affects the function of NodD, the expression of *nodA*, the first gene in the *nod* cluster, was measured. It was significantly enhanced by ESC treatment, which increased to a level equivalent to GEN induction (fig. 4H). Also, ESC largely saved the soybean plant according to plant height and fresh weight (fig. S8, G to I). After adding *S. fredii* to this system, we found that ESC did not affect the number of nodules but could increase the nitrogenase activity by about 2.3-fold before and after zoospore inoculation (Fig. 4I and fig. S8J). These findings demonstrate that ESC could be a potential agent for *P. sojae* prevention, which also promotes the symbiotic nitrogen fixation between rhizobium and soybean.

DISCUSSION

Bacterial chemotaxis plays an important role in human diseases, and the antibacterial medicine omeprazole might represent a proof-of-concept therapeutic by disorienting chemotactic bacteria (*1*). Since Zentmyer first reported zoospore chemotaxis for root exudates in 1961 (*3*, *24*), targeting chemoreceptors to block zoospore attraction has been considered a promising strategy for managing oomycete diseases (*2*). Previous research has shown that phenolic acids in maize root exudates inhibit soybean root and stem rot by repelling *P. sojae* zoospores (*25*). Likewise, the biocontrol bacterium *Burkholderia cepacia* remarkedly reduced the attractiveness of seed exudates to *Pythium* zoospores (*26*). However, oomycete chemoreceptors responsible for host attractants remain to be identified. Our results reveal that PsIRK1 is the receptor for GEN. ESC, a GEN analog, functions as an antagonist that attenuates zoospore chemotaxis and mitigates damping off caused by *P. sojae*. Given that zoospores are crucial for infection, this finding opens previously unexplored avenues for oomycete disease control by blocking chemoreceptors.

Plants use root-derived specialized metabolites to establish chemical communications with microbes in the rhizosphere to promote plant health (*27*, *28*). Soybean roots release GEN into rhizosphere to induce expression of nodulation (*nod*) genes in *Bradyrhizobium japonicum* and *S. fredii*, which is essential for *Rhizobium*-soybean symbiosis (*29*–*31*). Plants root exudates typically shape rhizosphere microbiomes to promote plant health (*27*, *32*). However, GEN also acts as a fatal signal by attracting the oomycete pathogen *P. sojae* to invade soybean (*2*). A total of 12 isoflavones were identified in soybean (*33*), among which DAI and GEN were found in the rhizosphere soil (*34*). Although GEN also functions as a phytoalexin to prevent pathogen attacks (*35*, *36*), it only results in 50% inhibition of *P. sojae* growth at 170 μM (*37*) and the major phytoalexins are glyceollins that are produced from DAI. Concentrations of DAI and GEN in the soybean rhizosphere would not exceed 10 μM (*34*, *38*). To counteract this, soybean promotes the conversion of DAI to glyceollin during infection to inhibit *P. sojae* growth, as it is unable to degrade the glyceollin (*39*). Therefore, transgenic soybean with enhanced content of glyceollin exhibits enhanced resistance to *P. sojae* (*40*). Here, we show that disrupting GEN-mediated *P. sojae* soybean chemotaxis by ESC can control the disease without adversely affecting *S. fredii*–mediated nodulation.

The zoospore homing sequence of *P. sojae* involves chemotaxis, encystment, cyst adhesion, germination, and germ-tube tropism (*41*), all of which can be triggered by isoflavones (*5*). Notably, chemotaxis, encystment, and germination triggered by isoflavones are impaired when *PsGPA1* is knockout or *PsGK4* is silenced (*10*), while *PsGPA1*^{5A}, *PsIRK1*, and *PsIRK2* mutants only appear impaired chemotaxis (table S2). These findings suggest that the PsIRK1-PsIRK2 complex regulates chemotaxis solely depending on G proteins. In contrast, plant RLKs and animal receptor tyrosine kinases (RTKs) usually transduce signals via both G protein–dependent and–independent pathways (*15*, *17*, *18*, *42*, *43*). Moreover, the PsIRK1-PsIRK2 complex and PsGK4 might synergistically regulate chemotaxis to isoflavones. Cross-communication or transactivation between GPCRs and RTKs, major classes of cell surface receptors in human and animals, is an important mechanism for diversifying signaling networks (*44*–*47*). Our investigations also provide the basis for the identification of how *P sojae* and other oomycete RLKs and GPCRs mediate the ethanol-triggered homing of zoospores to stressed roots.

MATERIALS AND METHODS

Chemicals and regents

GEN, DAI, and coumarins were purchased from MedChemExpress (Monmouth Junction, NJ, USA). All regents were dissolved in DMSO.

Strains and plants culture condition

The *P. sojae* WT strain P6497 and the knockout mutants used in this study was grown on 10% (v/v) V8 (Original VEGETABLE JUICE) agar medium at 25°C in the dark. The Δ*PsIRK1*, Δ*PsIRK2*, Δ*PsIRK3*, Δ*PsIRK4*, and Δ*PsIRK5* mutants, as reported in our previous study, were revived from slant cultures (*14*). *S. fredii* strain CCBAU45436 was cultured on tryptone-yeast extract (TY) agar medium at 28°C. *Nicotiana benthamiana* plants used for Co-IP assays were grown and maintained

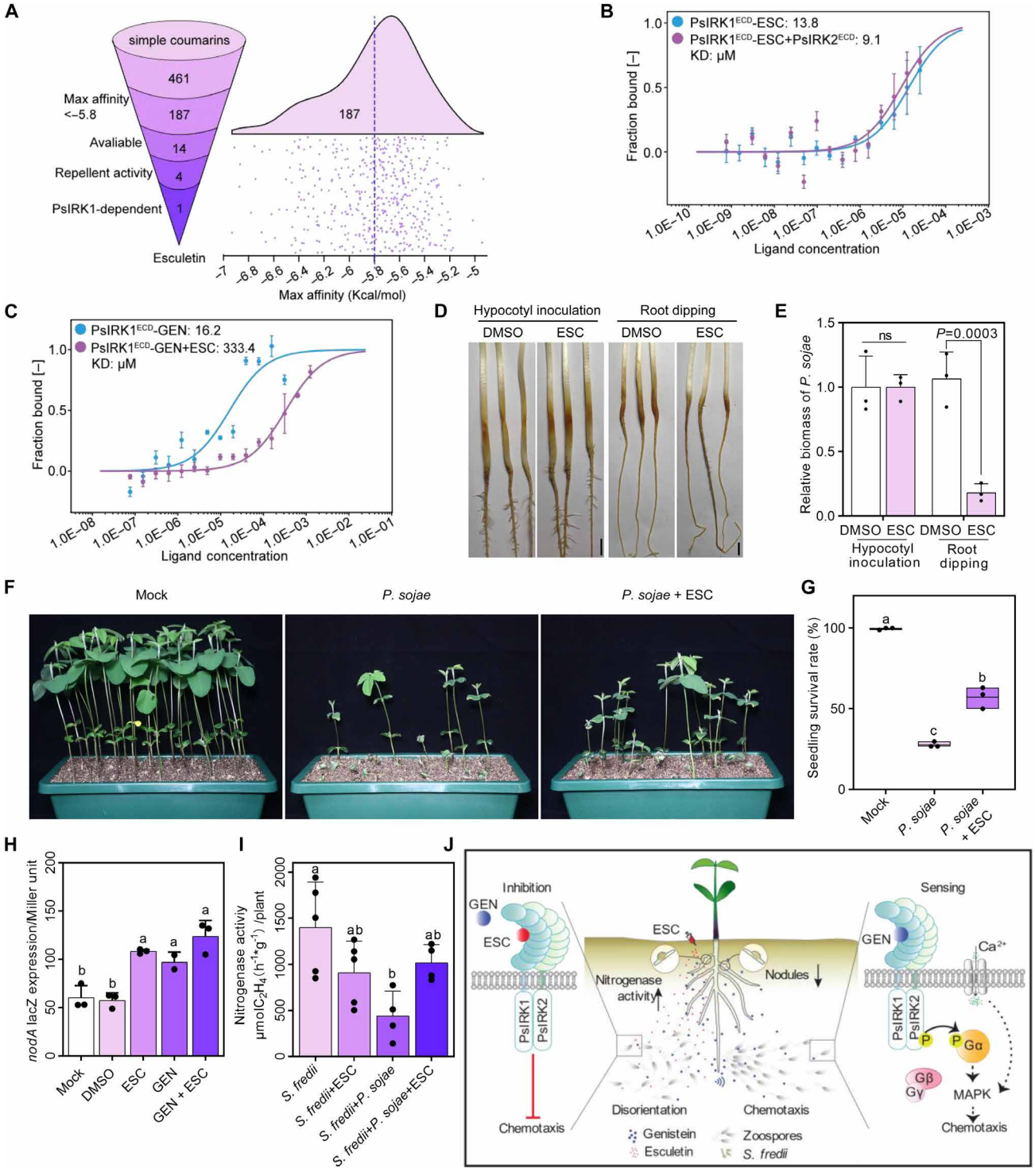

Fig. 4. Antagonist ESC prevents *P. sojae* infection by repelling zoospores. (**A**) Identification of the GEN antagonist by virtual screening. A total of 461 simple coumarins were selected for docking with PsIRK1^{ECD} using AutoDock Vina. (**B**) MST binding profiles of PsIRK1^{ECD} toward ESC, both before and after adding PsIRK2^{ECD}. (**C**) ESC disturbs the GEN-PsIRK1^{ECD} interaction in the MST assay. (**D**) ESC reduced *P. sojae* virulence due to disorientation of zoospores. Lesion lengths were photographed 48 hpi. Scale bars, 1 cm. (**E**) Relative biomass of the infected etiolated soybean hypocotyls ($n = 3$ biologically independent experiments). Two-tailed Student's *t* test was used. ns, not significant. $P = 0.0003$. Error bars indicate the mean fold changes with SD. (**F**) ESC prevents *P. sojae* infection in the pot experiment. Seedlings were pulled out after 4 days of cultivation in vermiculite, and the roots were immersed in a zoospore suspension pretreated with 100 μM ESC or DMSO for 30 min. The inoculated seedlings were transplanted into new pots, 30 seedlings per pot. Photographs were taken 14 dpi. Mock, seedlings without treatment. (**G**) Survival rates of soybean seedlings. The pot experiment was repeated three times. $n \geq 60$. (**H**) ESC induces the expression of *nodA* in *S. fredii* strain CCBAU45436. (**I**) Nitrogenase activity of *S. fredii* was not affected by ESC treatment. $n \geq 4$ biologically independent samples. Ordinary one-way ANOVA with Tukey's test was performed. Different letters represent classes with significant differences ($P < 0.05$). Error bars represent the mean fold changes with SD [(G), (H), and (I)]. (**J**) Proposed model of zoospore chemotaxis to GEN in *P. sojae*.

at 23°C, 60% relative humidity with an 8-hour photoperiod in environmentally controlled growth rooms. *Glycine max* (Hefeng47, a susceptible cultivar) used for virulence assays were planted in the vermiculite at 23°C with 60% relative humidity in the dark to obtain etiolated seedlings. For pot experiments, *G. max* was grown in darkness for 4 days before being inoculated and transplanted into new pots. The inoculated seedlings were planted 30 per pot at 23°C, 60% relative humidity, with an 8-hour photoperiod in the greenhouse.

Plasmid construction

Genomic DNA or cDNA from *P. sojae* were used as templates for polymerase chain reaction (PCR) amplification. Primers for fragment amplification are listed in table S1. The cloned genes for different assays were amplified using the Phanta Super-Fidelity DNA Polymerase (Vazyme) and verified by Sanger sequencing.

For the MST assay, the single-fragment homologous recombination method (Vazyme) was used to recombine $PsIRK1^{ECD}$, $PsIRK2^{ECD}$, $PsIRK3^{ECD}$, $PsIRK4^{ECD}$, and $PsIRK5^{ECD}$ into the pPICZαA vector, respectively. For *Agrobacterium*-mediated transient expression analysis, the cloned genes were inserted into the vector pCAMBIA1300-3×HA and pCAMBIA1300-3×Flag, respectively, with tags at the C terminus of the fusion protein. For prokaryotic expression, the relevant fragments were fused to the pGEX-6P (GST-tagged), pET28a (His-tagged), and pHMTc [maltose binding protein (MBP)–tagged] vectors.

To create Δ*PsIRK1/2* double-knockout transformants, Δ*PsGPA1* knockout transformants, and *PsGPA1* phosphorylation sites inactive transformants ($PsGPA1^{5A}$), vectors of two single guide RNAs (sgRNAs) and one homology-directed repair donor DNA were constructed for each. The sgRNAs were designed following the previous protocol (*48*, *49*). For Δ*PsGPA1* and Δ*PsIRK1/2* double-knockout mutant, the sgRNA fragment was ligated to pYF515 (G418) and pYF2.3 (oxathiapiprolin) using T4 DNA ligase (Vazyme), respectively. To produce donor DNA vector for Δ*PsIRK1/2* and Δ*PsGPA1*, the *mCherry* gene and flanking homology arm of 1 kb each were fused into the pBluescript SK II + vector using multiple fragment homologous recombination method (Vazyme). For $PsGPA1^{5A}$ transformants, the *PsGPA1* phosphorylation site and sgRNA site were synonymous substituted. The mutated *PsGPA1* sequence with two 1-kb fragments flanking the target gene were fused to pBluescript SK II + vector.

Generation of *P. Sojae* mutants

The mutants were generated following the PEG-$CaCl_2$–mediated protoplast transformation protocol (*47*). For Δ*PsIRK1/2* transformants, mycelium from the Δ*PsIRK2* mutant was used to generate protoplast. For Δ*PsGPA1* knockout transformants and $PsGPA1^{5A}$, mycelium of WT was used to produce protoplast. Transformants were screened using G418 (50 μg/ml) or oxathiapiprolin (0.05 μg/ml) (*49*). Genomic DNA from candidate transformants was extracted using the cetyl trimethylammonium bromide (CTAB) protocol. For Δ*PsIRK1/2* and Δ*PsGPA1* mutants, primer sets F1/R1 and F2/R2 (table S1) were used for PCR amplification, agarose gel electrophoresis, and Sanger sequencing. For the $PsGPA1^{5A}$ mutant, the expression level of *PsGPA1* was detected to ensure the gene was not silenced.

Growth rate, germination rate, virulence assay, and chemotaxis assay

To determine the growth rate, a diameter of 5-mm plug was grown on 10% V8 culture plates at 25°C in the dark for 6 days. Colony diameters were measured using software ImageJ, and the average growth rate was calculated (millimeter per day).

To produce zoospores, mycelium was repeatedly washed with sterilized tap water every 30 min until sporangium formed. Plates with 3 ml of water were kept at 25°C in the dark for 2 to 3 hours until zoospores produced. Zoospore suspension was collected for use. To detect cyst germination rate, zoospores were collected and resuspended gently using 5% V8 broth, shaken until encysted. After being kept at 25°C in the dark for 2 to 3 hours, 100-μl mixture was observed under microscope at 10× magnification. Number of cysts and germinated cysts in the visual field were measured, and the cyst germination rate was calculated as follows: germinated cysts / (cysts + germinated cysts). At least 20 visual fields were counted. For turning frequency, 10 random zoospores were traced to count turnaround times during 1 min (*11*).

For virulence assays, three methods were used. To determine the virulence of mutants, 4-day-old soybean etiolated seedlings were inoculated with ~200 zoospores or a 5-mm hyphal plug. To determine virulence decreased by chemotaxis, roots of 4-day-old etiolated seedlings were dipped for 30 min in zoospore suspension of 10^5/ml (*14*). Symptoms were evaluated and photographed at 48 hours postinoculation (hpi). Virulence was calculated by relative biomass, which was quantified by ratio of *P. sojae* DNA to *G. max* via relative quantitative PCR (SYBR qPCR Master Mix Kit, Vazyme). qPCR was performed using the QuantStudio 5 Real-time PCR System (96-well, Applied Biosystems, Thermo Fisher Scientific) following the manufacturer's instructions. The relative quantitative method ($2^{-\Delta\Delta Ct}$) was used to evaluate the quantitative variation. Primers used in qPCR are listed in table S1. All assays were repeated independently at least three times.

For chemotaxis assays, capillary tubes filled with an isoflavone solution were used to assess the chemotaxis *P. sojae* zoospores (*6*, *19*, *50*) (fig. S1). Five hundred microliters of 10^5/ml zoospore suspension was gently dropped onto the central depression of the slide. Capillary tubes were used to absorb soybean isoflavones with a concentration of 10 nM. Another end of the capillary tube was quickly overheated and sealed. The tube was dipped into the zoospore suspension for 6 min under a low-intensity light environment. The sample was placed under a microscope at 4× magnification and recorded with a charge-coupled device imaging system. The response of different isoflavones to chemotaxis was compared by counting the number of zoospores in the tube. The movies were speeded up by 45 times using the software Shotcut (https://shotcut.org/). Phenotypes of mutants tested in this study are summarized in table S2.

MST assay

For the MST assay, recombinant $PsIRK1^{ECD}$, $PsIRK2^{ECD}$, and $PsIRK3^{ECD}$ plasmids were introduced into *Pichia pastoris* strain GS115. The GS115 strain carrying the designated construct was cultured in buffered glycerol complex medium (BMGY) at 28°C for 5 days. The recombinant His-tagged proteins were isolated and purified using Ni–nitrilotriacetic acid (NTA) agarose beads. Each protein was labeled at a concentration of 10 μM using the MO-L001 Monolith Protein Labeling Kit RED-NHS (NanoTemper, Munich). The labeled proteins were subsequently mixed with varying concentrations of GEN or DAI in phosphate-buffered saline with Tween 20 buffer in accordance with the manufacturer's instructions. Ligand concentration ranged from 10 to 0.000305 μM. Measurements were conducted using the Monolith NT.115 instrument (NanoTemper) at

a temperature of 23.4°C, using 100% excitation power and 40% MST power. Data analysis to determine the interaction parameters was performed using MO Affinity Analysis version 2.3 software.

Interaction assays in vivo and in vitro

For Co-IP assays, leaves from 4-week-old *N. benthamiana* were syringe infiltrated with *Agrobacterium tumefaciens* strains GV3101 at optical density at 600 nm (OD_{600}) = 0.5. The strains were a mixture containing plasmid expressing 3× HA-tagged fusion protein and 3× Flag-tagged fusion protein. Thirty-six hours after infiltration, leaves were ground and homogenized in 1 ml of extraction buffer [150 mM NaCl, 1 mM EDTA, 25 mM tris-HCL (pH = 7.5), 10% (v/v) glycerol, 2% (v/v) PVP 40, 5‰ Triton X-100, and 0.1% (v/v) protease inhibitor cocktail (Roche, Mannheim)]. The homogenate was centrifuged at 15,000 rpm for 15 min at 4°C. A 5× SDS–polyacrylamide gel electrophoresis (PAGE) gel-loading buffer was added before boiled at 100°C. The protein expression was detected by Western blot using anti-Flag and anti-HA antibody following the dilution rate of 1:5000, visualized using a Multispectral Imaging System. After confirming the expression levels, proteins were incubated with 15 μl of Anti-HA-Tag Mouse mAb (Agarose Conjugated) (Abmart) for 4 hours. The beads were washed three times before adding 5× SDS-PAGE gel-loading buffer and boiling at 100°C for 8 min. The analysis was carried out by Western blot using anti-Flag and anti-HA antibody and shown with a Multispectral Imaging System. Ponceau S staining of the polyvinylidene difluoride (PVDF) membranes was used to verify equal loading. To determine the effect of GEN/DAI on the interaction between PsIRK1 and PsIRK2, 10 nM GEN/DAI was infiltrated 10 min before leaf harvesting, with the remaining steps of the Co-IP assay unchanged.

For GST pulldown assays, GST-tagged pGEX vectors and His-tagged pET28a `vectors were transformed into *Escherichia coli* Rosetta (DE3) strains to express prokaryotic proteins. Coomassie Blue (CBB) staining and Western blot were used to detect protein expression. Anti-GST and anti-His antibodies (Abmart) were used at a 1:5000 dilution, while goat anti-mouse IgG secondary antibody (IRDye 800CW, LicorBio) was used at a 1:10,000 dilution. The result was shown under an Infrared Imaging System (Odyssey CLx, LicorBio). Equal amount of GST-tagged protein was incubated with 25 μl of glutathione agarose beads (Glutathione Sepharose 4B, Millipore Sigma) for 2 hours at 4°C, then adding equal amount His-tagged proteins to co-incubate in the interaction system for another 5 hours at 4°C. The mixture was centrifuged and washed three times before adding 5× SDS-PAGE gel-loading buffer and boiled at 100°C. The samples were detected by Western blot with anti-His and anti-GST antibodies. GST-empty vector was used as negative control. To determine the effect of GEN/DAI on the interaction between PsIRK1 and PsIRK2, 10 nM GEN/DAI was added 30 min before the interaction progress ended. The remaining operation of the pull-down assay kept the same.

For size exclusion chromatography assay, purified GST-tagged $PsIRK1^{ECD}$ and $PsIRK2^{ECD}$ proteins were loaded into the high-performance liquid chromatograph to observe the retention time and peak height of each protein. Control samples included $PsIRK2^{ECD}$ + buffer (with a volume equal to $PsIRK1^{ECD}$) and $PsIRK1^{ECD}$ + buffer (with a volume equal to $PsIRK2^{ECD}$). $PsIRK2^{ECD}$ + $PsIRK1^{ECD}$ proteins were co-incubated with 10 nM GEN or DMSO at 4°C for 3 hours.

Ca^{2+} influx

Zoospores were treated with 10 nM GEN/DAI and 2 mM $CaCl_2$ for 5 min before collected and gently resuspended by ddH_2O. After washing twice, a final concentration of 5 μM Fluo-4 AM (Beyotime) was added. The samples were kept in 25°C in the dark for 30 min (*51*). Zoospores were washed by ddH_2O twice and resuspended with 1 ml of ddH_2O. The zoospores were kept in 25°C in the dark for 20 min before adding 200 μl each to a 96-well plate. The degree of Ca^{2+} influx was judged by fluorescence intensity at the excitation wave of 488 nm by GLOMAX96 microplate luminometer (Promega, Madison, WI). The single-cell fluorescence was examined under a Leica confocal laser scanning (TCS SP8, Leica Microsystem). Fluorescence intensity was analyzed using ZEN software.

MAPK assay

Zoospores were collected and frozen in liquid nitrogen after being exposed to 10 nM GEN/DAI for 0, 5, 10, 15 and 30 min to determine the optimal time for MAPK activation. The zoospores were resuspended with 100 μl of protein extraction buffer and shaken for 5 min (*52*). Total proteins were extracted and analyzed by SDS-PAGE and Western blots using rabbit anti–phospho-p44/p42 MAPK antibody (Cell Signaling Technology) at a 1:5000 dilution. The horseradish peroxidase (HRP) signal was detected using a Multispectral Imaging System. The PVDF membrane used for the Western blots was stained with Ponceau S to verify equal loading.

In vitro phosphorylation assay

The prokaryotic protein used for this assay was purified by Amylose resin (NEB) or Ni-NTA Agrose (Qiagen) depending on their tags. The expression level of purified proteins was assessed by CBB staining. A gradient concentration of BSA protein was used as a standard for sample concentration assessment. The assays were performed in a 20-μl mixture of protein kinase (~0.5 mg), substrate (~3 mg), or maltose binding protein (MBP, 3 mg) and kinase buffer [20 mM tris-HCl (pH 7.5), 10 mM $MgCl_2$, 1 mM $CaCl_2$, 100 mM adenosine 5′-triphosphate, 1 mM dithiothreitol]. For autophosphorylation activity reaction, ~3.5 mg of $PsIRK^{KD}$ was added to the reaction system. The reaction was incubated at 30°C for 30 min before terminated by mixing 5× SDS-PAGE gel-loading buffer with the sample and boiled at 100°C. The remaining steps followed the instructions of pIMAGO-biotin Phosphoprotein Detection on Western blot (800-10, TYMORA). The HRP signal was detected using a Multispectral Imaging System.

Virtual screening

To screen natural coumarins that inhibit GEN-induced chemotaxis, 2H-1-benzopyran-2-one were used as the key word to search the PubChem database. Criteria were set for our selection including the following: (i) molecular weight ranging from 100 to 300 g/mol; (ii) complexity ranging from 160 to 300; (iii) containing a maximum of 2 hydrogen bond donor atoms; and (iv) counts of hydrogen bond acceptors ranging from 2 to 5. A total of 461 simple coumarins were selected for virtual screening against $PsIRK1^{ECD}$. The molecular docking was performed with AutoDock Vina version 1.2.5 following the parameters: (i) the docking grid was centered at coordinates (x = −0.737, y = −1.245, z = −1.600), with a grid box size of (size_x = 72.851 Å, size_y = 50.155 Å, size_z = 101.947 Å); and (ii) the energy range was set to 5, the maximum number of docking

modes was set to 9, the exhaustiveness was set to 128, and the random seed was set to 2. After docking, hits with the max affinity less than −5.8 were selected. The commercially available molecules were bought for further chemotaxis assays.

Growth rate of *S. fredii*

S. fredii strain CCBAU45436 was cultured in TY liquid broth with the initial concentration of $OD_{600} = 0.001$. The strain was cultivated in an incubator shaker at 28°C. The value of OD_{600} was recorded every 6 hours until a plateau was reached. Six biological repeats were used in this assay.

Soybean fresh weight, height and nodulation

Overnight cultures of *S. fredii* were pelleted and resuspended in sterile water to reach an $OD_{600} = 1.0$. One hundred microliters of aliquot of bacterial suspension was used per plate to homogeneously inoculate the root of seedlings immediately. Plants were cultivated in a growth chamber at 28°C with a 16-hour photoperiod in the greenhouse. Fresh weight, height of the seedlings, and nodules were counted at 28 dpi.

Acetylene reduction assays

Assays were performed on individual plants as described previously (*53*). A single nodule-bearing soybean plant was placed into 20-ml glass vial containing little sterile water and closed with septa. Two milliliters of acetylene were injected per vial. Plants were incubated in growth chambers (28°C with light) for 2 hours (linear phase of ethylene production). One hundred milliliters of gas samples were analyzed on the gas chromatograph (Agilent 7890B). Activity was normalized to the incubation time.

Detection of nod gene expression level

To determine the effect of ESC on *S. fredii nodA* expression, the fusion plasmid pRA302-nodA was constructed transferred into the CCBAU45436 strain. GEN was used as a positive inducer. The expression of *nodA* was analyzed by measuring β-galactosidase activity.

Statistical analysis

Statistical significance was performed with Prism version 8.0.2.263. The logistic fitting curve was produced by OriginPro 2022.

Accession numbers

Genes used in this study can be found in the National Center for Biotechnology Information Nucleotide database: *PsIRK1* (MZ028045), *PsIRK2* (MZ028027), *PsIRK3* (MZ028039), *PsIRK4* (MZ028036), *PsIRK5* (MZ028032), and *PsGPA1* (EU652940).

Supplementary Materials

The PDF file includes:
Figs. S1 to S8
Legends for tables S1 to S3
Legends for movies S1 to S20

Other Supplementary Material for this manuscript includes the following:
Tables S1 to S3
Movies S1 to S20

REFERENCES AND NOTES

1. B. Zhou, C. M. Szymanski, A. Baylink, Bacterial chemotaxis in human diseases. *Trends Microbiol.* **31**, 453–467 (2023).
2. M. Kasteel, T. Ketelaar, F. Govers, Fatal attraction: How *Phytophthora* zoospores find their host. *Semin. Cell Dev. Biol.* **148-149**, 13–21 (2023).
3. G. A. Zentmyer, Chemotaxis of zoospores for root exudates. *Science* **133**, 1595–1596 (1961).
4. I. Bassani, M. Larousse, Q. D. Tran, A. Attard, E. Galiana, *Phytophthora* zoospores: From perception of environmental signals to inoculum formation on the host-root surface. *Comput. Struct. Biotechnol. J.* **18**, 3766–3773 (2020).
5. B. M. Tyler, *Phytophthora sojae*: Root rot pathogen of soybean and model oomycete. *Mol. Plant Pathol.* **8**, 1–8 (2007).
6. P. F. Morris, E. W. B. Ward, Chemoattraction of zoospores of the soybean pathogen, *Phytophthora sojae*, by isoflavones. *Physiol. Mol. Plant Pathol.* **40**, 17–22 (1992).
7. I. Comerford, S. R. McColl, Atypical chemokine receptors in the immune system. *Nat. Rev. Immunol.* **24**, 753–769 (2024).
8. D. Turrà, M. E. Ghalid, F. Rossi, A. D. Pietro, Fungal pathogen uses sex pheromone receptor for chemotropic sensing of host plant signals. *Nature* **527**, 521–524 (2015).
9. B. M. Tyler, S. Tripathy, X. Zhang, P. Dehal, R. H. Y. Jiang, A. Aerts, F. D. Arredondo, L. Baxter, D. Bensasson, J. L. Beynon, J. Chapman, C. M. B. Damasceno, A. E. Dorrance, D. Dou, A. W. Dickerman, I. L. Dubchak, M. Garbelotto, M. Gijzen, S. G. Gordon, F. Govers, N. J. Grunwald, W. Huang, K. L. Ivors, R. W. Jones, S. Kamoun, K. Krampis, K. H. Lamour, M. Lee, W. H. McDonald, M. Medina, H. J. G. Meijer, E. K. Nordberg, D. J. Maclean, M. D. Ospina-Giraldo, P. F. Morris, V. Phuntumart, N. H. Putnam, S. Rash, J. K. C. Rose, Y. Sakihama, A. A. Salamov, A. Savidor, C. F. Scheuring, B. M. Smith, B. W. S. Sobral, A. Terry, T. A. Torto-Alalibo, J. Win, Z. Xu, H. Zhang, I. V. Grigoriev, D. S. Rokhsar, J. L. Boore, *Phytophthora* genome sequences uncover evolutionary origins and mechanisms of pathogenesis. *Science* **313**, 1261–1266 (2006).
10. X. Yang, W. Zhao, C. Hua, X. Zheng, M. Jing, D. Li, F. Govers, H. J. G. Meijer, Y. Wang, Chemotaxis and oospore formation in *Phytophthora sojae* are controlled by G-protein-coupled receptors with a phosphatidylinositol phosphate kinase domain. *Mol. Microbiol.* **88**, 382–394 (2013).
11. C. Hua, Y. Wang, X. Zheng, D. Dou, Z. Zhang, F. Govers, Y. Wang, A *Phytophthora sojae* G-protein α subunit is involved in chemotaxis to soybean isoflavones. *Eukaryot. Cell* **7**, 2133–2140 (2008).
12. Z. Yin, D. Shen, Y. Zhao, H. Peng, J. Liu, D. Dou, Cross-kingdom analyses of transmembrane protein kinases show their functional diversity and distinct origins in protists. *Comput. Struct. Biotechnol. J.* **21**, 4070–4078 (2023).
13. A. Dievart, C. Gottin, C. Périn, V. Ranwez, N. Chantret, Origin and diversity of plant receptor-like kinases. *Annu. Rev. Plant Biol.* **71**, 131–156 (2020).
14. J. Si, Y. Pei, D. Shen, P. Ji, R. Xu, X. Xue, H. Peng, X. Liang, D. Dou, *Phytophthora sojae* leucine-rich repeat receptor-like kinases: Diverse and essential roles in development and pathogenicity. *iScience* **24**, 102725 (2021).
15. J. Xue, B. Gong, X. Yao, X. Huang, J.-F. Li, BAK1-mediated phosphorylation of canonical G protein alpha during flagellin signaling in *Arabidopsis*. *J. Integr. Plant Biol.* **62**, 690–701 (2020).
16. S. Pandey, Plant receptor-like kinase signaling through heterotrimeric G-proteins. *J. Exp. Bot.* **71**, 1742–1751 (2020).
17. S. R. Choudhury, S. Pandey, SymRK-dependent phosphorylation of Gα protein and its role in signaling during soybean (*Glycine max*) nodulation. *Plant J.* **110**, 277–291 (2022).
18. M. Ma, J. Zhou, X. Liang, Phosphorylation-dependent regulation of plant heterotrimeric G proteins: From activation to downstream signaling. *Sci. Bull.* **69**, 2967–2970 (2024).
19. B. M. Tyler, M. Wu, J. Wang, W. Cheung, P. F. Morris, Chemotactic preferences and strain variation in the response of *Phytophthora sojae* zoospores to host isoflavones. *Appl. Environ. Microbiol.* **62**, 2811–2817 (1996).
20. M. S. Connolly, N. Williams, C. A. Heckman, P. F. Morris, Soybean isoflavones trigger a calcium influx in *Phytophthora sojae*. *Fungal Genet. Biol.* **28**, 6–11 (1999).
21. W. R. H. Huang, C. Braam, C. Kretschmer, S. L. Villanueva, H. Liu, F. Ferik, A. M. van der Burgh, S. Boeren, J. Wu, L. Zhang, T. Nürnberger, Y. Wang, M. F. Seidl, E. Evangelisti, J. Stuttmann, M. H. A. J. Joosten, Receptor-like cytoplasmic kinases of different subfamilies differentially regulate SOBIR1/BAK1-mediated immune responses in *Nicotiana benthamiana*. *Nat. Commun.* **15**, 4339 (2024).
22. T. Minamikawa, T. Akazawa, I. Uritani, Isolation of esculetin from sweet potato roots with black rot. *Nature* **195**, 726–726 (1962).
23. C. Tian, Y. Zhou, Y. Zhang, Q. Li, Y. Zhang, D. Li, S. Wang, J. Wang, L. Gilbert, Y. Li, W. Chen, Comparative genomics of rhizobia nodulating soybean suggests extensive recruitment of lineage-specific genes in adaptations. *Proc. Natl. Acad. Sci. U.S.A.* **109**, 8629–8634 (2012).
24. G. A. Zentmyer, Attraction of zoospores of *Phytophthora cinnamomi* to avocado roots. *Calif. Avocado Soc.* **45**, 93–95 (1961).
25. H. Zhang, Y. Yang, X. Mei, Y. Li, J. Wu, Y. Li, H. Wang, H. Huang, M. Yang, X. He, S. Zhu, Y. Liu, Phenolic acids released in maize rhizosphere during maize-soybean intercropping inhibit *Phytophthora* blight of soybean. *Front. Plant Sci.* **11**, 886 (2020).
26. K. Heungens, J. L. Parke, Zoospore homing and infection events: Effects of the biocontrol bacterium *Burkholderia cepacia* AMMDR1 on two oomycete pathogens of pea (*Pisum sativum* L.). *Appl. Environ. Microbiol.* **66**, 5192–5200 (2000).

27. A. C. Huang, T. Jiang, Y. Liu, Y. Bai, J. Reed, B. Qu, A. Goossens, H. W. Nützmann, Y. Bai, A. Osbourn, A specialized metabolic network selectively modulates Arabidopsis root microbiota. *Science* **364**, eaau6389 (2019).
28. X. Wang, J. Zhang, X. Lu, Y. Bai, G. Wang, Two diversities meet in the rhizosphere: Root specialized metabolites and microbiome. *J. Genet. Genomics* **51**, 467–478 (2023).
29. R. M. Kosslak, R. Bookland, J. Barkei, H. E. Paaren, E. R. Appelbaum, Induction of *Bradyrhizobium japonicum* common nod genes by isoflavones isolated from *Glycine max*. *Proc. Natl. Acad. Sci. U.S.A.* **84**, 7428–7432 (1987).
30. R. F. Fisher, S. R. Long, *Rhizobium*–plant signal exchange. *Nature* **357**, 655–660 (1992).
31. C. Alías-Villegas, F. Fuentes-Romero, V. Cuéllar, P. Navarro-Gómez, M. J. Soto, J. Vinardell, S. Acosta-Jurado, Surface motility regulation of *Sinorhizobium fredii* HH103 by plant flavonoids and the NodD1, TtsI, NolR, and MucR1 symbiotic bacterial regulators. *Int. J. Mol. Sci.* **23**, 7698 (2022).
32. J. Sasse, E. Martinoia, T. Northen, Feed your friends: Do plant exudates shape the root microbiome? *Trends Plant Sci.* **23**, 25–41 (2018).
33. H. Wang, P. A. Murphy, Isoflavone content in commercial soybean foods. *J. Agric. Food Chem.* **42**, 1666–1673 (1994).
34. A. Sugiyama, Y. Yamazaki, S. Hamamoto, H. Takase, K. Yazaki, Synthesis and secretion of isoflavones by field-grown soybean. *Plant Cell Physiol.* **58**, 1594–1600 (2017).
35. R. A. Dixon, C. L. Steele, Flavonoids and isoflavonoids- a gold mine for metabolic engineering. *Trends Plant Sci.* **4**, 394–400 (1999).
36. H. Zhou, J. Lin, A. Johnson, R. L. Morgan, W. Zhong, W. Ma, *Pseudomonas syringae* type III effector HopZ1 targets a host enzyme to suppress isoflavone biosynthesis and promote infection in soybean. *Cell Host Microbe* **9**, 177–186 (2011).
37. L. I. Rivera-Vargas, A. F. Schmitthenner, T. L. Graham, Soybean flavonoid effects on and metabolism by *Phytophthora sojae*. *Phytochemistry* **32**, 851–857 (1993).
38. T. L. Graham, Flavonoid and isoflavonoid distribution in developing soybean seedling tissues and in seed and root exudates. *Plant Physiol.* **95**, 594–603 (1991).
39. A. V. Lygin, C. B. Hill, O. V. Zernova, L. Crull, J. M. Widholm, G. L. Hartman, V. V. Lozovaya, Response of soybean pathogens to glyceollin. *Phytopathology* **100**, 897–903 (2010).
40. Q. Cheng, N. Li, L. Dong, D. Zhang, S. Fan, L. Jiang, X. Wang, P. Xu, S. Zhang, Overexpression of soybean isoflavone reductase (*GmIFR*) enhances resistance to *Phytophthora sojae* in soybean. *Front. Plant Sci.* **6**, 1024 (2015).
41. J. W. Deacon, S. P. Donaldson, Molecular recognition in the homing responses of zoosporic fungi, with special reference to *Pythium* and *Phytophthora*. *Mycol. Res.* **97**, 1153–1171 (1993).
42. N. A. Kalogriopoulos, I. Lopez-Sanchez, C. Lin, T. Ngo, K. K. Midde, S. Roy, N. Aznar, F. Murray, M. Garcia-Marcos, I. Kufareva, M. Ghassemian, P. Ghosh, Receptor tyrosine kinases activate heterotrimeric G proteins via phosphorylation within the interdomain cleft of Gαi. *Proc. Natl. Acad. Sci. U.S.A.* **117**, 28763–28774 (2020).
43. X. Liang, P. Ding, K. Lian, J. Wang, M. Ma, L. Li, L. Li, M. Li, X. Zhang, S. Chen, Y. Zhang, J.-M. Zhou, *Arabidopsis* heterotrimeric G proteins regulate immunity by directly coupling to the FLS2 receptor. *eLife* **5**, 13568 (2016).
44. H. Daub, F. Weiss, C. Wallasch, A. Ullrich, Role of transactivation of the EGF receptor in signalling by G-protein-coupled receptors. *Nature* **379**, 557–560 (1996).
45. L. E. Kilpatrick, S. J. Hill, Transactivation of G protein-coupled receptors (GPCRs) and receptor tyrosine kinases (RTKs): Recent insights using luminescence and fluorescence technologies. *Curr. Opin. Endocr. Metab. Res.* **16**, 102–112 (2021).
46. T. W. Moody, L. Lee, I. Ramos-Alvarez, R. T. Jensen, Neurotensin receptors regulate transactivation of the EGFR and HER2 in a reactive oxygen species-dependent manner. *Eur. J. Pharmacol.* **865**, 172735 (2019).
47. R. Zhou, B. Han, C. Xia, X. Zhuang, Membrane-associated periodic skeleton is a signaling platform for RTK transactivation in neurons. *Science* **365**, 929–934 (2019).
48. Y. Fang, L. Cui, B. Gu, F. Arredondo, B. M. Tyler, Efficient genome editing in the oomycete *Phytophthora sojae* using CRISPR/Cas9. *Curr. Protoc. Microbiol.* **44**, 21A.1.1-21A.1.26 (2017).
49. W. Wang, Z. Xue, J. Miao, M. Cai, C. Zhang, T. Li, B. Zhang, B. M. Tyler, X. Liu, *PcMuORP1*, an oxathiapiprolin-resistance gene, functions as a novel selection marker for *Phytophthora* transformation and CRISPR/Cas9 mediated genome editing. *Front. Microbiol.* **10**, 2402 (2019).
50. P. F. Morris, E. Bone, B. M. Tyler, Chemotropic and contact responses of *Phytophthora sojae* hyphae to soybean isoflavonoids and artificial substrates. *Plant Physiol.* **117**, 1171–1178 (1998).
51. R. Zhou, Y. Chen, S. Li, X. Wei, W. Hu, S. Tang, J. Ding, W. Fu, H. Zhang, F. Chen, W. Hao, Y. Lin, R. Zhu, K. Wang, L. Dong, Y. Zhao, X. Feng, F. Chen, C. Ding, W. Hu, TRPM7 channel inhibition attenuates rheumatoid arthritis articular chondrocyte ferroptosis by suppression of the PKCα-NOX4 axis. *Redox Biol.* **55**, 102411 (2022).
52. Y. Pei, P. Ji, J. Si, H. Zhao, S. Zhang, R. Xu, H. Qiao, W. Duan, D. Shen, Z. Yin, D. Dou, A *Phytophthora* receptor-like kinase regulates oospore development and can activate pattern-triggered plant immunity. *Nat. Commun.* **14**, 4593 (2023).
53. F. Berrabah, M. Bourcy, A. Cayrel, A. Eschstruth, S. Mondy, P. Ratet, B. Gourion, Growth conditions determine the DNF2 requirement for symbiosis. *PLOS ONE* **9**, e91866 (2014).

Acknowledgments: We thank B. Tyler and X. Liang for fruitful discussions during preparing the manuscript. **Funding:** This study was supported by grants from the National Natural Science Foundation of China (32472502 and 32202251 to Z.Y., 32230089 to D.D., 32372493 to D.S., and 32302309 to Y.B.), the Natural Science Foundation of Jiangsu Province (BK20221000 to Z.Y.), the Fundamental Research Funds for the Central Universities (KYQN2023039 to Z.Y.), the China Agriculture Research System (CARS-21 to D.D.), the Guidance Foundation, the Sanya Institute of Nanjing Agricultural University (NAUSY-MS14 to D.D.), and the Graduate Research Innovation Program of Jiangsu Province (KYCX23_0815 to P.J.). **Author contributions:** D.D. and Z.Y. conceived and designed the research. P.J., Y.B., H.Z., Y.P., W.S., K.O., Z.Q., J.S., Z.Z., and D.S. performed experiments. P.J., Y.B., and Z.Y. analyzed data. X.X. and H.T. performed the virtual screening. P.J., Z.Y., and D.D. wrote the manuscript. All authors read and approved the final manuscript. **Competing interests:** The authors declare that they have no competing interests. **Data and materials availability:** All data needed to evaluate the conclusions in the paper are present in the paper and/or the Supplementary Materials.

Submitted 11 September 2024
Accepted 3 December 2024
Published 8 January 2025
10.1126/sciadv.adt0925